

Shearlet-Based Edge Detection: Flame Fronts and Tidal Flats

Emily J. King^{a,b}, Rafael Reisenhofer^a, Johannes Kiefer^c, Wang-Q Lim^d, Zhen Li^e, Georg Heygster^e

^a Center for Industrial Mathematics, University of Bremen, Bremen, Germany;

^b Institute for Algebra, Geometry, Topology and Their Applications, University of Bremen, Bremen, Germany;

^c Department of Production Engineering, University of Bremen, Bremen, Germany;

^d Image & Video Coding Group, Fraunhofer Institute for Telecommunications – Heinrich Hertz Institute (Fraunhofer HHI);

^e Institute of Environmental Physics, University of Bremen, Bremen, Germany

ABSTRACT

Shearlets are wavelet-like systems which are better suited for handling geometric features in multi-dimensional data than traditional wavelets. A novel method for edge and line detection which is in the spirit of phase congruency but is based on a complex shearlet transform will be presented. This approach to detection yields an approximate tangent direction of detected discontinuities as a byproduct of the computation, which then yields local curvature estimates.

Two applications of the edge detection method will be discussed. First, the tracking and classification of flame fronts is a critical component of research in technical thermodynamics. Quite often, the flame fronts are transient or weak and the images are noisy. The standard methods used in the field for the detection of flame fronts do not handle such data well. Fortunately, using the shearlet-based edge measure yields good results as well as an accurate approximation of local curvature. Furthermore, a modification of the method will yield line detection, which is important for certain imaging modalities.

Second, the Wadden tidal flats are a biodiverse region along the North Sea coast. One approach to surveying the delicate region and tracking the topographical changes is to use pre-existing Synthetic Aperture Radar (SAR) images. Unfortunately, SAR data suffers from multiplicative noise as well as sensitivity to environmental factors. The first large-scale mapping project of that type showed good results but only with a tremendous amount of manual interaction because there are many edges in the data which are not boundaries of the tidal flats but are edges of features like fields or islands. Preliminary results will be presented.

Keywords: edge detection, line detection, shearlets, phase congruency, flame fronts, tidal flat, synthetic aperture radar

1. INTRODUCTION

Edge detection is a common subfield of image processing. Numerous methods have been presented through the years, some better than others. In this paper, we present a novel method of edge detection that uses ideas from both shearlet-based image processing and phase congruency. This method yields approximations of tangent directions and local curvature as well. Edges are not the only kinds of discontinuities which appear in images. One may wish to detect lines of varying pixel thickness not as a region bounded by two edges but as a uniform line. A slight modification of the edge detection algorithm will yield line detection.

In the 1970's and 80's planar imaging techniques emerged which revolutionized laser combustion diagnostics by providing spatially correlated information taken at a speed fast enough to catch transient features due to turbulence.¹⁻⁴ Determining the geometry of the flame front yields important information about combustion. This often achieved using a binarization technique^{5,6} or an approximation of the local intensity gradient.^{7,8} In binarization techniques, a intensity filter is applied to the image to obtain a binary image, where the flame and

Send correspondence to Rafael Reisenhofer, reisenhofer@math.uni-bremen.de.

non-flame pixels hopefully take different values. Then the edge is the boundary between the two regions. Gradient approximation techniques include numerous well-known techniques from Canny⁹ to wavelet-based^{10,11} and even shearlet-based¹² techniques. The basic idea is that after some sort of preprocessing, like smoothing with a Gaussian kernel, the pixelwise gradient is approximated and thresholded. The preprocessing and thresholding techniques can be fine-tuned in various manners. Neither of these types of techniques handle line detection well. However, when short-lived radicals like CH and HCO are imaged using PLIF (planar laser-induced fluorescence¹³), the flame front appears as a line rather than an edge. We shall show that our method performs well for both tasks of line detection and edge detection in noisy real-life data. Furthermore, information about local geometry is also yielded.

The Wadden Sea is an intertidal region along the southeastern portion of the North Sea bordering Denmark, Germany, and the Netherlands. “Wad” is Dutch for mud flat, which encompasses much of the Wadden Sea. The geography of the region is in constant flux, due to natural and anthropogenic reasons. Like many wetlands, the region hosts biodiversity while also being very delicate. The Danish, German, and Dutch governments have been collaborating since 1978 to conserve the area, which was also named a UNESCO World Heritage site in 2009. Tracking topological changes to the region is of utmost importance to its conservation. One approach to tracking the changes is to use apply segmentation and edge detection techniques to the massive amount of preexisting Synthetic Aperture Radar (SAR) data of the region.^{14–16} However, SAR imaging suffers from speckle noise and is also highly susceptible to environmental changes. For example, the relative darkness of land and sea changes when it is very windy. Due to this, the previous work involved massive amount of manual interaction making it not feasible to broadly apply. We will present some very preliminary results showing the superiority of the shearlet-based edge detection method over the wavelet-based method previously used.

The basic ideas behind the edge- and line-detecting method will be presented in Section 2. Then applications of the method to flame front detection and mud flat tracking will be shown in Section 3

2. METHOD

The core idea of the method first appeared in¹⁷ and is essentially that phase congruency should be modified to use the strength of the shearlet transform, namely its anisotropic nature. In order to make it work well with real data, the algorithm has since been strengthened and fine-tuned, for example, by adding line detection and local curvature estimation. Expanded analysis of the application to flame front detection will be published in¹⁸ while a more in-depth description of the mathematics behind the algorithm will appear in¹⁹. The corresponding author may be contacted in order to obtain the code. Here we will explain the basics of phase congruency and shearlets and how they work together to yield information about edges and lines.

2.1 Shearlets

Wavelets rose to prominence in the 1980’s. There are countless good references about wavelet theory, like.^{20,21} A typical (dyadic, discrete, one-dimensional) wavelet system is of the form

$$\left\{ \psi_{2^n, 2^{-n}k} := 2^{n/2} \psi(2^n (\cdot - 2^{-n}k)) = 2^{n/2} \psi(2^n \cdot - k); \quad n, k \in \mathbb{Z} \right\}.$$

Since the dilation by 2^n changes the essential support of the wavelet ψ and the translation by k moves around these dilated versions of ψ , looking at the inner products $\langle f, \psi_{a,t} \rangle$ for $a > 0$ yields local, multiscale information about a function f at location t . This is in contrast to the Fourier coefficients $\langle f, e^{2\pi i k \cdot} \rangle$, which give periodic information about f . Wavelets have proven to be very useful in numerous applications, even image processing, where 2-dimensional systems are often formed by a tensor-like construction. For example, the JPEG2000 compression scheme is based on wavelets.²² However, the isotropic nature of wavelet systems means that one is not able to extract any directional information about features in $2D$. Essentially, wavelets are fantastic for 1-dimensional data but are not optimal for 2-dimensional data. A number of approaches have been suggested over the past decade, like curvelets,²³ ridgelets,²⁴ contourlets,²⁵ bandlets,²⁶ wedgelets,²⁷ and shearlets,^{28–30} with the goal of extracting geometric information from 2- and higher dimensional data. Shearlets have a beautiful underlying mathematical theory, being built using unitary representations of certain classes of groups,^{31–36} that the other systems lack. Furthermore, shearlets have many nice properties, like nearly optimally approximating so-called

cartoon-like images^{37, 38} and having an associated multi-resolution analysis like wavelets.³⁹ However, the most important selling point is that the implementation of shearlets – unlike any of the other systems – is both open source and actively being developed.⁴⁰ Shearlets are very similar to wavelets, except that the isotropic dilation of wavelets is replaced with anisotropic dilation and shearing – a nicer-to-implement substitution for rotation, namely

$$\left\{ \psi_{a,s,t} := a^{3/4} \psi(S_s A_a(\cdot - t)); t \in \mathbb{R}^2, a > 0, s \in \mathbb{R} \right\},$$

where for $a > 0$

$$A_a = \begin{pmatrix} a & 0 \\ 0 & \sqrt{a} \end{pmatrix},$$

is the *parabolic scaling matrix* and for $s \in \mathbb{R}$

$$S_s = \begin{pmatrix} 1 & s \\ 0 & 1 \end{pmatrix},$$

the *shearing matrix*. In order to prevent directional bias in necessarily finite implementations, *cone-adapted shearlets* are used.²⁸ The standard *cone-adapted shearlet system* $\mathcal{SH}(\phi, \psi, \tilde{\psi})$ generated by $\phi \in L^2(\mathbb{R}^2)$ and $\psi, \tilde{\psi} \in L^2(\mathbb{R}^2)$ is the union of

$$\{\phi_k := \phi(\cdot - k); k \in \mathbb{Z}^2\} \text{ (low frequency component),}$$

$$\left\{ \tilde{\psi}_{2^n, \ell, (S_\ell A_{2^n})^{-1}k} = 2^{3n/4} \psi(S_\ell A_{2^n} \cdot -k); n \geq 0, |\ell| \leq \lceil 2^{n/2} \rceil, k \in \mathbb{Z}^2 \right\}, \text{ (horizontal cone) and}$$

$$\left\{ \tilde{\psi}_{2^n, \ell, (\tilde{S}_\ell \tilde{A}_{2^n})^{-1}k} = 2^{3n/4} \tilde{\psi}(\tilde{S}_\ell \tilde{A}_{2^n} \cdot -k); n \geq 0, |\ell| \leq \lceil 2^{n/2} \rceil, k \in \mathbb{Z}^2 \right\} \text{ (vertical cone),}$$

where

$$\tilde{A}_a = \begin{pmatrix} \sqrt{a} & 0 \\ 0 & a \end{pmatrix} \text{ and } \tilde{S}_\ell = S_\ell^T.$$

Sometimes this system is modified along the “seams” by projecting the horizontal and vertical cone systems so that they do not overlap. We, however, do not do that. A cone-adapted shearlet system induces a tiling of the frequency domain that looks almost polar, see Figure 1. We actually employ a finer discretization of the shearlet

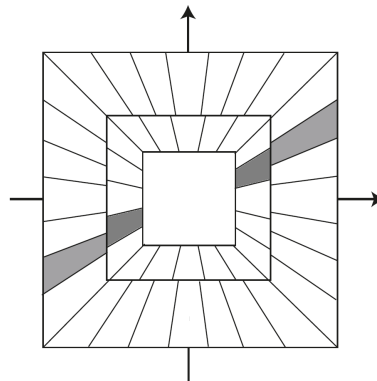


Figure 1. Tiling of the frequency domain generated by the essential frequency support of a classical cone-adapted shearlet system. Source: Gitta Kutyniok, TU Berlin

system in our edge detection method, but the essential idea is the same. See¹⁹ for more information. We end this section by modifying a shearlet construction to create complex shearlets, which still yield local geometric information but have certain desirable traits that Fourier bases also have.^{17, 41} In particular, we would like real part of the generating function to be even-symmetric (like cosine) and the imaginary part odd-symmetric (like sine). In order to do this, we employ the Hilbert transform,

$$H(f)(t) = \lim_{a \rightarrow \infty} \int_{-a}^a \frac{f(\tau)}{t - \tau} d\tau.$$

Loosely speaking, the Hilbert transform switches the roles of sine and cosine, and, in general, it turns an even-symmetric function into an odd-symmetric function and vice versa. If $\psi^{(e)}$ is a real-valued, even-symmetric shearlet, then we define the *complex shearlet* to be

$$\psi = \psi^{(e)} + i\psi^{(o)} := \psi^{(e)} + iH(\psi^{(e)}),$$

with $\tilde{\psi}(x_1, x_2) = \psi(x_2, x_1)$. We will construct $\psi^{(e)}$ as a tensor product of the Mexican hat wavelet and a Gaussian. There is a similar construction of complex wavelets^{42–44}, which we will use for illustrative purposes in the following section.

2.2 Phase congruency and the new method

Phase congruency is an edge detection algorithm originally based on Fourier coefficients^{45,46} and then extended to a contrast-invariant measure using complex wavelets in.^{47,48} For brevity and simplicity, we will describe a one dimensional edge detection algorithm which is an improvement of the approach in.^{47,48} The shearlet version is a straight forward generalization of this method and may be found in.^{17–19} The key idea is to note for a complex wavelet ψ what the inner products $\langle f, \psi_{a,t}^{(e)} \rangle$ and $\langle f, \psi_{a,t}^{(o)} \rangle$ look like when a varies over the positive numbers and the shift of t centers the wavelets at a jump discontinuity. To make the pattern clearer, we will normalize the $\psi_{a,t}^{(e)}$ and $\psi_{a,t}^{(o)}$ such that they have L^1 -norm 1. We model the perfect one-dimensional edge as the function $f = 10\mathbb{1}_{[-\infty, 0.5)} - 10\mathbb{1}_{[0.5, \infty)}$, where $\mathbb{1}_A$ is the characteristic function that takes the value 1 on A and 0 on the complement of A . We can see what various wavelet coefficients look like when the wavelets are

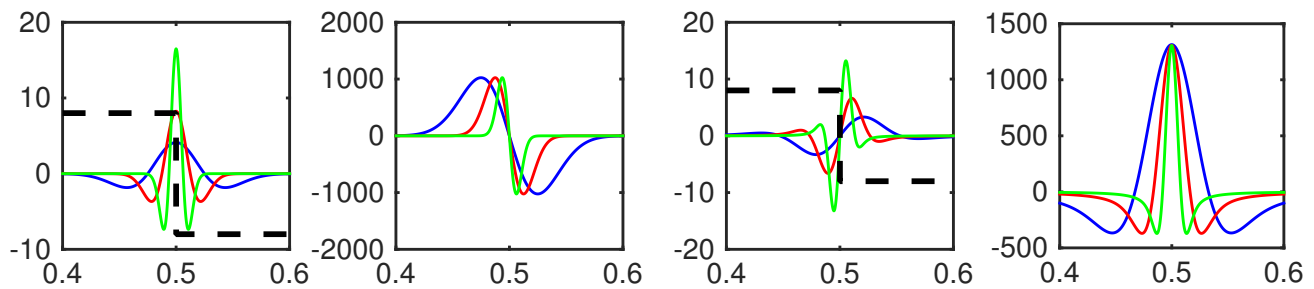


Figure 2. From left to right. (a) $\psi_{a,1/2}^{(e)}$, dilations of the even-symmetric wavelet centered on the edge. (b) A graph of the wavelet coefficients of the different dilated even-symmetric wavelets at different positions. The horizontal axis is the shift y and the vertical axis is the value of $\langle f, \psi_{a,y}^{(e)} \rangle$. (c) $\psi_{a,1/2}^{(o)}$, dilations of the odd-symmetric wavelet centered on the edge. (d) A graph of the wavelet coefficients of the different dilated odd-symmetric wavelets at different positions. The horizontal axis is the shift y and the vertical axis is the value of $\langle f, \psi_{a,y}^{(o)} \rangle$.

perfectly centered on the jump discontinuity in Figure 2. Figure 2(a) shows $\psi_{a,1/2}^{(e)}$ for three different values of $a > 0$ overlaying the edge function f . The graph in Figure 2(b) shows the values of $\langle f, \psi_{a,t}^{(e)} \rangle$ for the three values of $a > 0$ plotted against the values of t . We can see across scales that the inner product vanishes when the even-symmetric wavelets are centered at the edge and quickly grows in absolute value when moving away from the edge. Similarly, Figure 2(c) shows $\psi_{a,1/2}^{(o)}$ for the same three values of $a > 0$. In Figure 2(d), we can see that the coefficients $\langle f, \psi_{a,t}^{(o)} \rangle$ not only have a local maximum at $t = 1/2$, but the same maximum value. We present now an edge measure, which yields a value between 0 and 1 measuring “edge-ness” of a location. That is, a measure of 0 means that there is no edge at the location and 1 means that there certainly is. We make use of the three traits noticed in the test case. Namely, that when t_0 is the location of a jump discontinuity, that

- for each $a > 0$, $\langle f, \psi_{a,t_0}^{(e)} \rangle = 0$,
- for each $a > 0$, $\langle f, \psi_{a,t}^{(o)} \rangle$ achieves a local maximum at $t = t_0$, and
- for all $a > 0$, $\langle f, \psi_{a,t_0}^{(o)} \rangle = C$ for some nonzero constant C .

The original papers essentially just leverage the fact that $\langle f, \psi_{a,t_0}^{(e)} \rangle / \langle f, \psi_{a,t_0}^{(o)} \rangle$ is constant across scales when t_0 is the location of a jump discontinuity. The hope is, by balancing the three different traits against each other that the resulting measure will be robust to both noise and discretization, which seems to be the case in practice. This leads to the definition of the one-dimensional edge measure E .

Definition 1. Given a pair of even-symmetric and odd-symmetric wavelets $\psi^{(e)}$ and $\psi^{(o)}$ which satisfy certain hypotheses (in particular, an L^1 -normalized Mexican hat wavelet and its Hilbert transform works) and parameters $J \in \{1, 2, \dots\}$, positive dilations $\{a_j\}_{j \in \{1, 2, \dots, J\}}$ and a very small $\epsilon > 0$, we define for a 1D signal f

$$\tilde{E}(y) = \frac{\left| \sum_{j=1}^J \langle f, \psi_{a_j, y}^{(o)} \rangle \right| - \sum_{j=1}^J \left| \langle f, \psi_{a_j, y}^{(e)} \rangle \right|}{J \max_{j \in \{1, 2, \dots, J\}} \left| \langle f, \psi_{a_j, y}^{(o)} \rangle \right| + \epsilon},$$

and

$$E(y) = \max\{\tilde{E}(y), 0\}.$$

In one-dimension, a perfect line is represented by a delta function. Notice that in this idealized case,

- for each $a > 0$, $\langle \delta_{t_0}, \psi_{a,t_0}^{(o)} \rangle = 0$, and
- for each $a > 0$, $\langle \delta_{t_0}, \psi_{a,t}^{(e)} \rangle$ achieves a local maximum at $t = t_0$.

Given appropriate normalization, one can also obtain for all $a > 0$, $\langle \delta_{t_0}, \psi_{a,t_0}^{(e)} \rangle = C$ for some nonzero constant C . Essentially, in order to detect lines versus edges, one simply switches the role of the even- and odd-symmetric wavelets. In practice, one needs to be a bit more careful than in the edge detection case, since “lines” in a quantized, discrete image could be 1-, 2-, 3- or more pixels thick. On the other hand, “edges” in a quantized, discrete image can be viewed as falling “between pixels.” When detecting lines, it is thus important to estimate the thickness of the line first. For more details, see.¹⁹ The essential idea behind the generalization of the edge- and line-measures to 2D using complex shearlets is to first loosely approximate the orientation s^* of a potential edge. This is done by finding which pair of parameters (a, s) yields the largest coefficients of $\left| \langle f, \psi_{a,s,t_0}^{(o)} \rangle \right|$ for a fixed t_0 over a fixed range of a and all of the s computed. Then an edge- or line-measure is computed in much the same way as in the 1D case, but along the preferred orientation s^* .

2.3 Post-processing

We end this section by discussing a few details of how the results are fine-tuned. First, the measure presented in the preceding subsection yields a value between 0 and 1. Thus, a thresholding scheme must be applied in order to get a binary decision of whether or not a pixel lies on an edge or line. We simply directly threshold with a user-given value, although certainly more advanced methods like hysteresis, which is employed in the Canny method⁹ could be used. Then after the simple thresholding, a thinning procedure, specifically the thinning option of `bwmorph` in the Matlab Image Processing Toolbox, is applied.⁴⁹

When detecting edges (resp., lines) we already have an estimate of the orientation s^* from the direction of the largest odd-symmetric (resp., even-symmetric) coefficients. While this yields a fairly nice approximation of the tangent direction of an edge, it is not nearly exact enough for local curvature estimation. To get around this, we employ two methods in conjunction. Namely, we consider not just the largest coefficient but the largest coefficient and the two coefficients which neighbor it in terms of the shear parameter and think of them as sample points of a concave down parabola in order to estimate where the “true” maximum value is located. In order to do this, we are using the methods of subpixel extrema extraction as proposed in.⁵⁰ Further, a conversion between the shearing directions and rotation directions is computed. Once a more precise estimate of the tangent directions of the thinned edge or line has been computed, the local curvature is found using the central difference estimate of the derivative.

2.4 Overview of the method

The basic idea of the method is as follows.

Input: Image f , real-valued even-symmetric shearlet $\psi^{(e)}$, various parameters.

1. Compute ψ using the Hilbert transform and $\tilde{\psi}$ by switching the variables.
2. Compute $\langle f, \psi_{a,s,t} \rangle$ for certain values of (a, s) at each pixel t .
3. At each pixel t , estimate the preferred direction of a possible edge/line.
4. At each pixel t , compute an edge/line measure by comparing the values of the even- and odd-symmetric shearlet coefficients in the preferred direction. If doing line detection, also estimate the line thickness.
5. Threshold the edge/line measure.
6. Thin the edge measure.
7. Calculate local first and second derivatives, if desired.

3. APPLICATIONS

3.1 Flame front detection

For the task of flame front detection, we demonstrate the capabilities of the complex shearlet-based edge measure by processing a noisy mock image designed to represent the characteristics of typical flame data, a PLIF visualization of long-lived OH radicals as well as a PLIF visualization of short-lived CH radicals. In the case of the mock image (see Figure 3), the values of the shearlet-based edge measure are plotted alongside all post-processing steps, namely thresholding and thinning, estimation of local tangent orientations and estimation of local curvature. For the image of OH radicals, where flame fronts are represented by edges, and the visualization of CH radicals, where flame fronts are represented by lines, only the thinned flame fronts and estimates of the tangent orientation are shown (see Figure 4). All of the pre-processed images in this section are from the lab of Johannes Kiefer.

For an in-depth evaluation and comparison to other edge and line detection techniques, see.¹⁸

3.2 Tidal flats

Here we present a very preliminary example of the superiority of the shearlet-based (phase congruency-inspired) edge detection method in picking up the borders of a tidal flat in the Wadden Sea to the use of a wavelet-based (gradient-approximating) edge detection method, coupled with denoising and diffusion-based segmentation, as was used in.¹⁶ Figure 5 contains a comparison of the complex-shearlet-based edge detection method to the combination of wavelet-based edge detection with denoising and segmentation. In the image, we see a waterway bounded on the top by farmland. The dark areas in the image are the features of interest, the mud flats.

A section of the original image is enlarged in Figure 6. One can see on the left-hand-side that the wavelet-based method (shown in red) picks up a lot of noise in the waterway as edges, as well as many of the land features. On the right-hand-side, one sees the edges picked up by the complex-shearlet method. The method picks up most of the tidal flat edges running near the top, including the small “island” in the upper right-hand corner, and the piece of the tidal flat in the lower right corner, while managing to not pick up too many false positives. Unlike with the wavelet-based methods, the only other preprocessing applied to the image before the shearlet-based method was used was simply taking the logarithm as non-precise way of turning multiplicative noise into additive noise. It should be mentioned that getting results like these requires a different tuning of the parameters of the shearlet-based method than what was used in Section 3.1. These parameters are available on request.

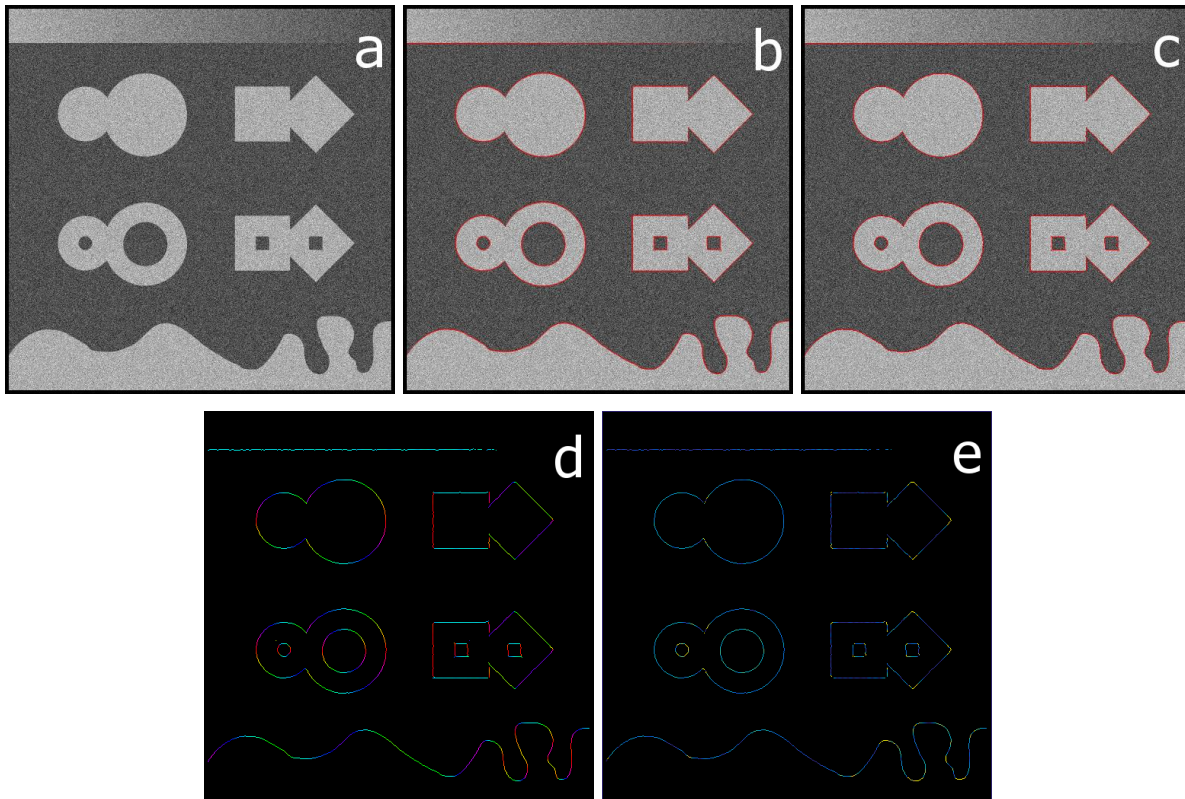


Figure 3. (a) Mock image perturbed by additive Gaussian noise. (b) The brightness of red corresponds to the local value of the complex shearlet-based edge measure. (c) The red lines are obtained from thresholding and thinning the output of the shearlet-based edge measure, depicted in the previous image. (d) Color-coded estimates of the local tangent orientation, where light blue indicates a perfectly horizontal and red represents a perfectly vertical orientation. (e) Color-coded estimates of the local curvature, where dark blue denotes zero curvature and yellow indicates a curvature greater or equal than 5° .

4. CONCLUSION

The complex shearlet edge measure works well on noisy, real-life data. A few examples of flame front and tidal flat boundary detection were presented here which look good, but thorough numerical experiments^{18]} give more quantitative evidence of the success. The method works quite well on flame front data but still requires more work via the addition of further image processing procedures like sophisticated handling of the speckle noise and a powerful segmentation algorithm in order to completely automate the task of determining the boundaries of tidal flats. Unlike many other edge detection algorithms, this approach can be easily modified to detect lines, which appear in experimental data, for example, certain flame fronts. Furthermore, the anisotropic nature of shearlets allows the method to give local geometric information of edges and lines, like tangent and curvature.

ACKNOWLEDGEMENTS

Emily J. King was supported in part by an AMS-Simons travel grant and Zentrum für Forschungsförderung der Uni Bremen Explorationsprojekt “Hilbert Space Frames and Algebraic Geometry.”

REFERENCES

- [1] Dyer, M. J. and Crosley, D. R., “Two-dimensional imaging of OH laser-induced fluorescence in a flame,” *Optics Letters* **7**, 382–384 (1982).

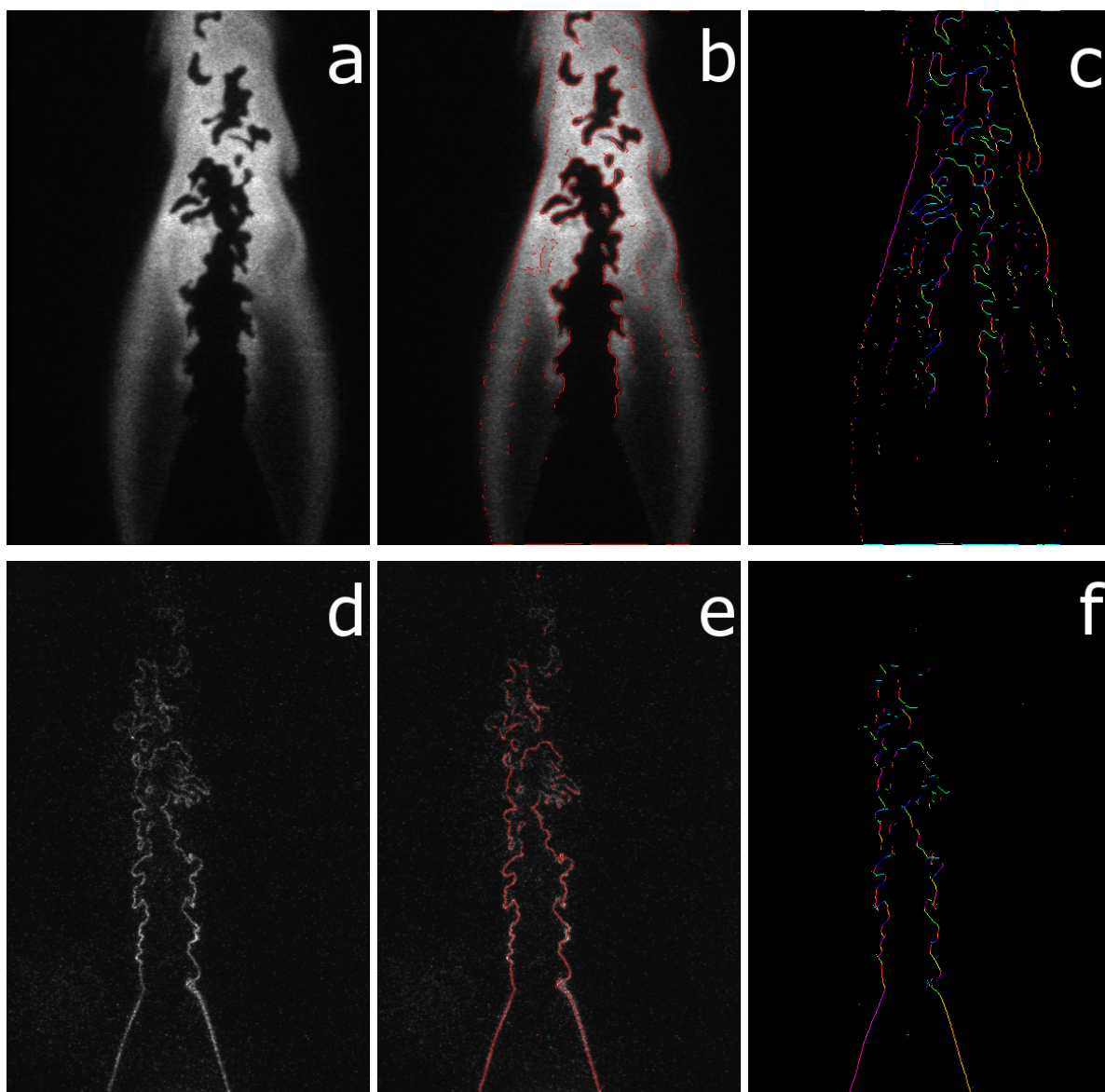


Figure 4. (a) PLIF visualization of long-lived OH radicals. (b) Thresholded and thinned output of the shearlet-based edge measure. (c) Color-coded estimates of the local tangent orientation, where light blue indicates a perfectly horizontal and red represents a perfectly vertical orientation. (d) PLIF visualization of short-lived CH radicals. (e) Thresholded and thinned output of the shearlet-based line measure. (f) Color-coded estimates of the local tangent orientation, where light blue indicates a perfectly horizontal and red represents a perfectly vertical orientation.

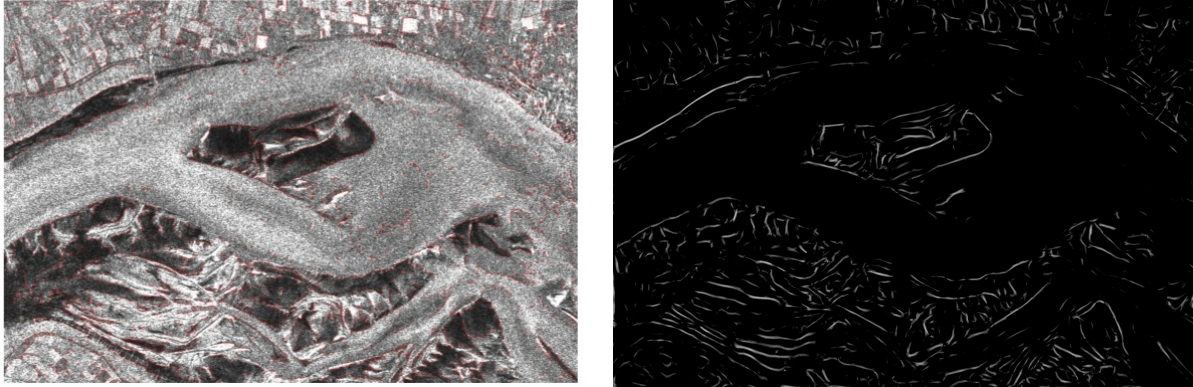


Figure 5. Left: Previously used automatic method (simple wavelet-based edge detection + diffusion-based segmentation) before manual labor. Right: Complex-shearlet-based edge detection without diffusion or denoising.

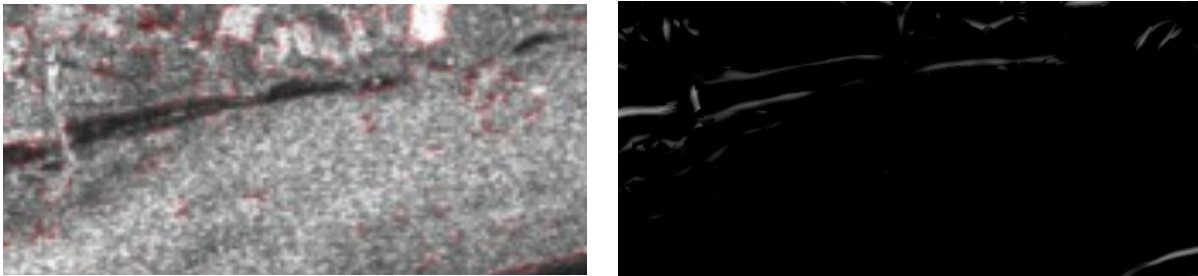


Figure 6. Left: Previously used automatic method (simple wavelet-based edge detection + diffusion-based segmentation) before manual labor. Right: Complex-shearlet-based edge detection without diffusion or denoising.

- [2] Fourchette, D. C., Zurn, R. M., and Long, M. B., "Two-dimensional rayleigh scattering thermometry in a turbulent nonpremixed methane-hydrogen flame," *Combustion Science and Technology* **44**, 307–317 (1986).
- [3] Aldén, M., Bood, J., Li, Z., and Richter, M., "Visualization and understanding of combustion processes using spatially and temporally resolved laser diagnostic techniques," *Proceedings of the Combustion Institute* **33**, 69–97 (2011).
- [4] Thurow, B., Jiang, N., and Lempert, W., "Review of ultra-high repetition rate laser diagnostics for fluid dynamic measurements," *Measurement Science and Technology* **24**, 012002 (2013).
- [5] Kiefer, J., Li, Z. S., Zetterberg, J., Bai, X. S., and Alden, M., "Investigation of local flame structures and statistics in partially premixed turbulent jet flames using simultaneous single-shot CH and OH planar laser-induced fluorescence imaging," *Combustion and Flame* **154**, 802–818 (2008).
- [6] Haq, M. Z., Sheppard, C. G. W., Wooley, R., Greenhalgh, D. A., and Lockett, R. D., "Wrinkling and curvature of laminar and turbulent premixed flames," *Combustion and Flame* **131**, 1–15 (2002).
- [7] Slabaugh, C. D., Pratt, A. C., and Lucht, R. P., "Simultaneous 5 kHz OH-PLIF/PIV for the study of turbulent combustion at engine conditions," *Applied Physics B* **118**, 109–130 (2015).
- [8] Bayley, A. E., Hardalupas, Y., and Taylor, A. M. K. P., "Local curvature measurements of a lean, partially premixed swirl-stabilised flame," *Experiments in Fluids* **52**, 963–983 (2012).
- [9] Canny, J., "A computational approach to edge detection," *IEEE Transactions on Pattern Analysis and Machine Intelligence* **8**(6), 679–698 (1986).
- [10] Mallat, S. and Hwang, W. L., "Singularity detection and processing with wavelets," *IEEE Trans. Inf. Theory* **38**, 617–643 (Mar. 1992).
- [11] Mallat, S. and Zhong, S., "Characterization of signals from multiscale edges," *IEEE Trans. Pattern Anal. Mach. Intell.* **14**, 710–732 (Jul. 1992).
- [12] Yi, S., Labate, D., Easley, G. R., and Krim, H., "A shearlet approach to edge analysis and detection," *IEEE Transactions on Image Processing* **18**(5), 929–941 (2009).

- [13] Sweeney, M. and Hochgreb, S., “Autonomous extraction of optimal flame fronts in OH planar laser-induced fluorescence images,” *Applied Optics* **48**, 3866–3877 (2009).
- [14] Heygster, G., Dannenberg, J., and Notholt, J., “Topographic mapping of the German tidal flats analyzing SAR images with the waterline method,” *IEEE Trans. Geosci. Remote Sens.* **48**, 1019–1030 (March 2010).
- [15] Dannenberg, J., *Ableitung der Topographie des Wattenmeeres aus ERS-SAR Daten*, PhD thesis, Univ. of Bremen, Bremen, Germany (2004). German.
- [16] Li, Z., *Morphological Development of the German Wadden Sea from 1996 to 2009 Determined with the Waterline Method and SAR and Landsat Satellite Images*, PhD thesis, Uni Bremen, Bremen, Germany (2014).
- [17] Reisenhofer, R., *The Complex Shearlet Transform and Applications to Image Quality Assessment*, Master’s thesis, Technische Universität Berlin (2014).
- [18] King, E. J., Kiefer, J., and Reisenhofer, R., “Shearlet-based detection of flame fronts,” in preparation (2015).
- [19] King, E. J. and Reisenhofer, R., “Complex shearlet-based edge detection,” In preparation (2015).
- [20] Daubechies, I., [*Ten lectures on wavelets*], vol. 61 of *CBMS-NSF Regional Conference Series in Applied Mathematics*, Society for Industrial and Applied Mathematics (SIAM), Philadelphia, PA (1992).
- [21] Heil, C. and Walnut, D. F., eds., [*Fundamental papers in wavelet theory*], Princeton University Press, Princeton, NJ (2006).
- [22] Taubman, D. and Marcellin, M., “JPEG2000: standard for interactive imaging,” *Proceedings of the IEEE* **90**(8), 1336–1357 (2002).
- [23] Candès, E. J. and Donoho, D. L., “New tight frames of curvelets and optimal representations of objects with piecewise C^2 singularities,” *Comm. Pure Appl. Math.* **57**(2), 219–266 (2004).
- [24] Candès, E. J. and Guo, F., “New multiscale transforms, minimum total variation synthesis: applications to edge-preserving image reconstruction,” *Signal Processing* **82**(11), 1519 – 1543 (2002).
- [25] Do, M. N. and Vetterli, M., “Contourlets,” in [*Beyond wavelets*], Welland, G. V., ed., *Studies in Computational Mathematics* **10**, 1–27, Academic Press/Elsevier Science, San Diego, CA (2003).
- [26] Pennec, E. L. and Mallat, S., “Bandelet image approximation and compression,” *SIAM Journal of Multiscale Modeling and Simulation* **4**, 2005 (2005).
- [27] Donoho, D. L., “Wedgelets: nearly minimax estimation of edges,” *Ann. Statist.* **27**(3), 859–897 (1999).
- [28] Guo, K., Kutyniok, G., and Labate, D., “Sparse multidimensional representations using anisotropic dilation und shear operators,” in [*Wavelets und Splines*], und M. J. Lai, G. C., ed., 189–201, Nashboro Press, Nashville, TN (2006).
- [29] Kutyniok, G. and Labate, D., “Resolution of the wavefront set using continuous shearlets,” *Trans. Amer. Math. Soc.* **361**(5), 2719–2754 (2009).
- [30] Kutyniok, G., Labate, D., Lim, W.-Q., and Weiss, G., “Sparse multidimensional representation using shearlets,” in [*Wavelets XI*], Papadakis, M., Laine, and Unser, eds., *Society of Photo-Optical Instrumentation Engineers (SPIE) Conference Series* **5914**, 254–262 (aug 2005).
- [31] Dahlke, S., Kutyniok, G., Steidl, G., and Teschke, G., “Shearlet coorbit spaces and associated Banach frames,” *Appl. Comput. Harmon. Anal.* **27**(2), 195–214 (2009).
- [32] Dahlke, S., Steidl, G., and Teschke, G., “The continuous shearlet transform in arbitrary space dimensions,” in [*Structured Decompositions and Efficient Algorithms*], Dahlke, S., Daubechies, I., Elad, M., Kutyniok, G., and Teschke, G., eds., *Dagstuhl Seminar Proceedings*(08492), Schloss Dagstuhl - Leibniz-Zentrum fuer Informatik, Germany, Dagstuhl, Germany (2009).
- [33] Dahlke, S. and Teschke, G., “The continuous shearlet transform in higher dimensions: variations of a theme,” in [*Group Theory: Classes, Representation and Connections, and Applications*], Danellis, C. W., ed., *Mathematics Research Developments*, Nova Publishers (2010).
- [34] King, E. J., *Wavelet and frame theory: frame bound gaps, generalized shearlets, Grassmannian fusion frames, and p -adic wavelets*, PhD thesis, University of Maryland, College Park (2009).
- [35] Czaja, W. and King, E. J., “Isotropic shearlet analogs for $L^2(\mathbb{R}^k)$ and localization operators,” *Numer. Funct. Anal. Optim.* **33**(7-9), 872–905 (2012).
- [36] Czaja, W. and King, E. J., “Anisotropic shearlet transforms for $L^2(\mathbb{R}^k)$,” *Math. Nachr.* **287**(8-9), 903–916 (2014).

- [37] Kutyniok, G. and Lim, W.-Q., "Shearlets on bounded domains," in [*Approximation Theory XIII: San Antonio 2010*], **12**, 187–206, Springer (2012).
- [38] Grohs, P. and Kutyniok, G., "Parabolic molecules," *Found. Comput. Math.* **14**, 299–337 (April 2014).
- [39] Kutyniok, G. and Sauer, T., "Adaptive directional subdivision schemes and shearlet multiresolution analysis," *SIAM J. Math. Anal.* **41**, 1436–1471 (2009).
- [40] "Shearlab." www.shearlab.org. Accessed: 2015-7-15.
- [41] Storath, M., *Amplitude and sign decompositions by complex wavelets - Theory and applications to image analysis*, PhD thesis, Technische Universität München (2013).
- [42] Kingsbury, N., "Image processing with complex wavelets," *Philosophical Transactions of the Royal Society of London* **357**(1760), 2543–2560 (1999).
- [43] Selesnick, I. W., "Hilbert transform pairs of wavelet bases," *IEEE Signal Processing Letters* **8**(6), 170–173 (2001).
- [44] Selesnick, I. W. and Abdelnour, A. F., "Symmetric wavelet tight frames with two generators," *Applied and Computational Harmonic Analysis* **17**(2), 211–225 (2004).
- [45] Morrone, M. C. and Owens, R. A., "Feature detection from local energy," *Pattern Recognition Letters* **6**, 303–313 (1987).
- [46] Morrone, M. C., Ross, J., Burr, D. C., and Owens, R., "Mach bands are phase dependent," *Nature* **324**(6094), 250–253 (1986).
- [47] Kovesi, P., "Phase congruency: A low-level image invariant," *Psychological Research* **64**, 136–148 (2000).
- [48] Kovesi, P., "Image features from phase congruency," *Videre: Journal of Computer Vision Research* **1**(3), 1–26 (1999).
- [49] Lam, L., Lee, S. W., and Suen, C. Y., "Thinning Methodologies - A Comprehensive Survey," *IEEE Transactions on Pattern Analysis and Machine Intelligence* **14**, 879 (Sep. 1992).
- [50] Bailey, D. G., "Sub-pixel estimation of local extrema," in [*Proceedings of Image and Vision Computing New Zealand*], 414–419 (Nov. 2003).